Pacific Basin tsunami hazards associated with mass flows in the Aleutian arc of Alaska

Christopher F. Waythomas [a],[*], Philip Watts [b], Fengyan Shi [c], James T. Kirby [c]

[a] US Geological Survey, Alaska Science Center, Alaska Volcano Observatory, 4230 University Drive, Suite 201, Anchorage, AK 99508, USA
[b] Applied Fluids Engineering, Inc., 6216 E. Pacific Coast Highway, PMB 237, Long Beach, CA 90803, USA
[c] University of Delaware, Dept. of Civil and Environmental Engineering, Center for Applied Coastal Research, Newark, DE 19716, USA

ARTICLE INFO

ABSTRACT

We analyze mass-flow tsunami generation for selected areas within the Aleutian arc of Alaska using results from numerical simulation of hypothetical but plausible mass-flow sources such as submarine landslides and volcanic debris avalanches. The Aleutian arc consists of a chain of volcanic mountains, volcanic islands, and submarine canyons, surrounded by a low-relief continental shelf above about 1000–2000 m water depth. Parts of the arc are fragmented into a series of fault-bounded blocks, tens to hundreds of kilometers in length, and separated from one another by distinctive fault-controlled canyons that are roughly normal to the arc axis. The canyons are natural regions for the accumulation and conveyance of sediment derived from glacial and volcanic processes. The volcanic islands in the region include a number of historically active volcanoes and some possess geological evidence for large-scale sector collapse into the sea. Large scale mass-flow deposits have not been mapped on the seafloor south of the Aleutian Islands, in part because most of the area has never been examined at the resolution required to identify such features, and in part because of the complex nature of erosional and depositional processes. Extensive submarine landslide deposits and debris flows are known on the north side of the arc and are common in similar settings elsewhere and thus they likely exist on the trench slope south of the Aleutian Islands. Because the Aleutian arc is surrounded by deep, open ocean, mass flows of unconsolidated debris that originate either as submarine landslides or as volcanic debris avalanches entering the sea may be potential tsunami sources.

To test this hypothesis we present a series of numerical simulations of submarine mass-flow initiated tsunamis from eight different source areas. We consider four submarine mass flows originating in submarine canyons and four flows that evolve from submarine landslides on the trench slope. The flows have lengths that range from 40 to 80 km, maximum thicknesses of 400–800 m, and maximum widths of 10–40 km. We also evaluate tsunami generation by volcanic debris avalanches associated with flank collapse, at four locations (Makushin, Cleveland, Seguam and Yunaska SW volcanoes), which represent large to moderate sized events in this region. We calculate tsunami sources using the numerical model TOPICS and simulate wave propagation across the Pacific using a spherical Boussinesq model, which is a modified version of the public domain code FUNWAVE. Our numerical simulations indicate that geologically plausible mass flows originating in the North Pacific near the Aleutian Islands can indeed generate large local tsunamis as well as large transoceanic tsunamis. These waves may be several meters in elevation at distal locations, such as Japan, Hawaii, and along the North and South American coastlines where they would constitute significant hazards.

Published by Elsevier Ltd.

1. Introduction

Tsunami initiated by gravity driven mass flows of unconsolidated debris are increasingly recognized as important coastal hazards in many parts of the world (Keating and McGuire, 2000; Lee et al., 2003; Watts et al., 2005). Several recent tsunami disasters have been attributed to mass-flow tsunami sources (e.g., Tappin

* Corresponding author. Tel.: +1 907 786 7122.
E-mail address: chris@usgs.gov (C.F. Waythomas).

et al., 2001, 2008), and many seismic events that produce tsunamis may also trigger tsunamigenic landslides (Lander and Lockridge, 1989). Although the mechanism of tsunami generation by both subaerial and submarine mass flows has been studied for some time, it is only recently that models capable of integrating the source, propagation and inundation components of a tsunami event have become available for application to hazard evaluation.

In this context, we examine the mass-flow tsunami potential of the Aleutian arc of Alaska (Fig. 1), a region known for its great subduction zone earthquakes and related tsunamis, but little known for its ability to produce tsunamigenic mass flows. We evaluate two types of tsunamigenic mass flows: mobile, long-runout submarine landslides, and volcanic debris avalanches that originate from large-scale volcanic flank failures. We want to know if these mass flows can produce potentially hazardous tsunamis within the Pacific Ocean basin. Although we do not present a detailed hazard evaluation for the modeled waves, we show the approximate scale of events required to produce trans-Pacific waves.

The Aleutian arc is a major volcanic island arc that is the result of subduction along the Aleutian trench. It forms the northern rim of the Pacific Ocean basin and extends from the Kamchatka Peninsula in Russia some 3000 km eastward to upper Cook Inlet (Fig. 1). Magma generation and Quaternary volcanism within the arc have produced a number of large, high relief stratocones oriented along a northeast-southwest axis that roughly parallels the axis of the trench.

At least 40 volcanoes in the Aleutian arc have erupted in the past 250 years and another 20 volcanoes have been active in the Holocene (Simkin and Siebert, 1994; Miller et al., 1998; Schaefer and Nye, 2002). The frequency of eruptions and number of large calderas of Holocene age (Miller and Smith, 1987) indicates that this is a magmatically active volcanic arc.

Most of the arc is remote and sparsely populated, and many volcanic processes that typically constitute hazards in other volcanic regions pose are less significant here because of limited population and infrastructure. However, much of the arc is surrounded by deep ocean, and mass flows of unconsolidated debris that enter or initiate on the sea floor of the North Pacific Ocean or Bering Sea have the potential to initiate tsunamis that could affect other parts of coastal Alaska as well as coastlines around the Pacific Rim far from this region (Waythomas and Watts, 2003; Fryer et al., 2004). Although other volcanic processes, such as explosively generated ash clouds, are important local and regional hazards and should not be discounted, mass-flow tsunami generation in relation to volcanic and tectonic activity in the Aleutian arc has not been described, and except for a few locations, potential tsunami hazards associated with volcanic activity in the region are not well

known (Waythomas and Neal, 1998; Waythomas et al., 2003a,b; Waythomas and Watts, 2003).

The purpose of this paper is to consider the physical setting of the Aleutian arc in the context of a potential source region for mass-flow initiated tsunamis and to present an analysis and numerical simulations of large mass-flow initiated tsunamis that reach coastlines around the Pacific Rim. We find that submarine landslides, similar in size to those known in other continental margin settings and having volumes of about 160 km^3 or larger, can produce trans-Pacific tsunamis that could be hazardous to coastal areas around the Pacific Rim. Large volcanic debris avalanches at island volcanoes also produce waves, but because the volumes are smaller relative to the submarine mass flows we simulate, the resulting waves also are smaller and the degree of potential hazard in the Pacific basin is less.

2. Physical setting of the Aleutian arc

The Aleutian arc extends westward from Cook Inlet on the east (approximately 61° N, 152° W) to Attu Island (52° 56.997′ N, 172° 35.331′ E). Buldir Island, about 200 km east of Attu (Fig. 2), is the westernmost island with known subaerial Holocene volcanism (Wood and Kienle, 1990). In the eastern part of the arc, the plate convergence vector is approximately 90 degrees to the trench axis and rates are about 7.5 cm/year. To the west, the convergence vector becomes more oblique and rates decline to about 2.5 cm/year, and eventually all of the motion in the western part of the arc becomes strike-slip (Engebretson et al., 1985). In the eastern part of the arc, volcanoes have developed on the continental crust and are situated 300–500 km north of the trench (Jacob et al., 1977), whereas those in the central to western part of the arc grew from largely submarine environments and are situated within 200 km of the trench. In general, the areas where convergence is most rapid also correspond to regions with the greatest magmatic output as indicated by volcano volume and frequency of historical eruptions (Fournelle et al., 1994).

Previous studies have subdivided the Aleutian arc into two geologically distinct segments, the Aleutian Ridge segment to the west, and the Alaska Peninsula–Kodiak Island segment to the east (Vallier et al., 1994). The Aleutian Ridge includes the Aleutian Islands and numerous submerged volcanic mountains and submarine canyons that are surrounded by a low-relief shelf above about 1000–2000 m water depth (Fig. 1) (Scholl et al., 1987).

The Aleutian Ridge is fragmented into a series of discrete fault-bounded blocks, each block being tens to hundreds of kilometers in length (Geist et al., 1988). The blocks are separated from one another by distinctive fault-controlled canyons that are roughly normal to the main axis of the Aleutian trench. The canyons are

Fig. 1. Location of the Aleutian arc in the North Pacific Ocean basin and setting of the Aleutian Islands and Alaska Peninsula.
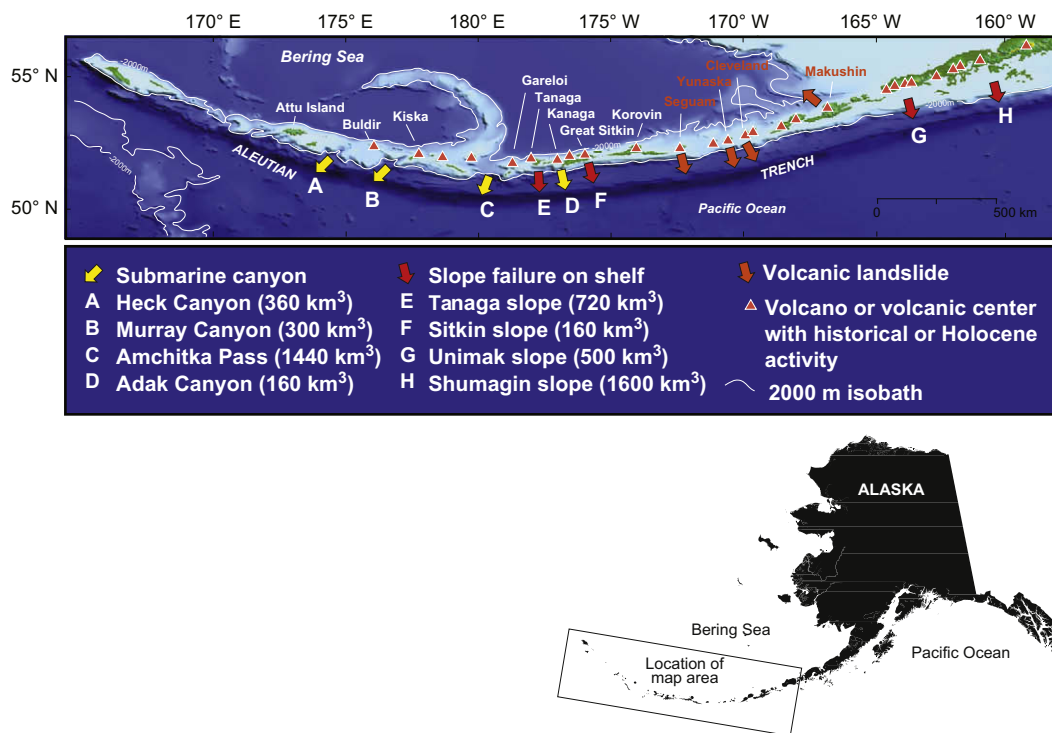
Fig. 2. Bathymetric map of the central and western Aleutian arc showing location of mass flow tsunami sources and volumes. Bold arrows indicate direction of flow path and initial propagation direction of tsunami.

important regions for the accumulation and conveyance of sediment derived from glaciation and volcanic process at nearby islands.

The bathymetry of the Aleutian arc is dominated by the Aleutian trench, the deepest part of which is about 7600 m below sea level. Landward of the trench is a series of horst and graben-like features, called the Aleutian terrace, that extend from about 4500 m depth to about 1000 m depth. Parts of the terrace are tilted gently north and the area is generally an accumulation zone for volcaniclastic and glaciomarine deposits (Dobson et al., 1996). The water depth over the Aleutian terrace and the submarine canyons that cross the trench slope is >200 m (Fig. 2).

During the last glacial maximum, ca 20–18 ka, glacier ice extended southward across the Aleutian shelf and into Cook Inlet as the sea level fell to about −125 m (Manley and Kaufman, 2002). Although little is known about the character of glacial deposits on the shelf, bathymetric maps of the area indicate extensive zones of ice stagnation drift and moraine. Eruptions at Aleutian arc volcanoes throughout the late Pleistocene and Holocene have occurred in the presence of ice and snow, and this has led to the generation of volcanic mudflows or lahars. These flows reached the sea and contributed volcaniclastic debris to the shelf. Studies of sediment provenance and dispersal south of the Aleutian arc indicate that sand layers of Holocene age recovered from piston cores taken from the trench slope (e.g. DSDP core 186 shown in Fig. 6) consist primarily of volcaniclastic debris derived from volcanic sources (Underwood, 1986a,b). The sand layers, some of which are several meters thick, are interpreted as to have formed from gravity driven sediment flows that were funneled through submarine canyons. Sediment-gravity-flow deposits accumulated on the slope north of the trench or extended beyond the trench-slope break (Underwood, 1986a,b; Underwood and Hathon, 1989) and clearly indicate the potential for long-runout submarine mass flows in this area. Although we cannot be certain that all such sediment gravity flows

originated from large submarine landslides, it is reasonable to assume that some of them did.

Deposits of unconsolidated volcaniclastic and glacial debris on the shelf and trench slope, and the submarine topography of the Aleutian arc in general, make this region a suitable environment for the generation of submarine mass flows as in other parts of Alaska (Hampton and Bouma, 1977; Schwab and Lee, 1983; Carlson et al., 1991; Karl and Carlson, 1996; Hampton et al., 1996) and in similar marine environments elsewhere (Locat and Mienert, 2003). Thus, we hypothesize that the trench slope along the south flank of the Aleutian arc is a likely source region for tsunamigenic mass flows.

A remaining physical characteristic of the region is its numerous subduction zone earthquakes, some of which are among the largest ever recorded (Taber et al., 1991; Haeussler and Plafker, 2003). Large earthquakes are a well-known mechanism for initiating mass failures of various types (Keefer, 1984, 2002), and subduction zone earthquakes in the Aleutian arc have triggered submarine landslides in several areas (Wilson and Torum, 1972; Fryer et al., 2004; Lee et al., 2006).

3. Submarine mass-flow tsunami sources

Submarine mass flows of unconsolidated sediment are an acknowledged generation mechanisms for tsunamis (Ward, 2001; Lee et al., 2003; Watts et al., 2003, 2005; Grilli and Watts, 2005; Harbitz et al., 2006; Tappin et al., 2008). As a result of these and other studies, the hazards posed by mass-flow initiated waves are widely recognized as important local hazards, and should also be regarded as significant regional hazards. We suggest that the Aleutian Islands region (Fig. 1) is an area capable of producing tsunamigenic mass flows, and here we present first-order evaluations of hypothetical, but plausible, mass-flow triggered tsunamis

that originate in the Aleutian Islands and propagate across the Pacific Ocean.

We evaluate submarine mass-flow initiated tsunamis in eight distinct source areas within the central and western Aleutian arc (Fig. 2). The dimensions and characterization of the submarine mass flows are dictated by the geology and morphology of each source area (Table 1) and are typical of submarine mass flows that have occurred in continental slope settings elsewhere, including Alaska (Edgers and Karlsrud, 1982; Coleman and Prior, 1988; Hampton et al., 1996; Piper and McCall, 2003; Fryer et al., 2004; McMurtry et al., 2004; von Huene et al., 2004; McAdoo and Watts, 2004; Solheim et al., 2005).

The tsunami sources we evaluate are generic submarine mass flows with an assumed specific density of 1.85, initial lengths of 40–80 km, maximum thicknesses of 400–800 m, and maximum widths of 10–40 km (Table 1). The mass flows initiate in water 2000–3000 m deep and flow generally southward along the sea floor toward the Aleutian trench (Fig. 2). The dimensions given in Table 1 vary with margin shape and slope, whereas the ratios of dimensions stay the same. As described in Watts et al. (2003,

2005) submarine mass flows exhibit minimal basal friction and undergo translational acceleration over long distances (tens to hundreds of kilometers). Although we have not identified specific submarine mass-flow deposits or features south of the Aleutian arc having the geometry described in Table 1, documented tsunamigenic submarine landslides in other parts of the world (Table 2) are of similar size. Submarine mass-flow deposits have been identified in GLORIA imagery of the seafloor of the southern Bering Sea basin north of the Aleutian arc (Groome et al., 1997). Individual deposits in this area are $>3 \times 10^4$ km^2 although their volumes are unknown.

4. Subaerial mass-flow tsunami sources

We evaluate tsunami generation by subaerial mass flows in the context of large volcanic flank failures and associated debris avalanches entering the North Pacific Ocean and Bering Sea. Our approach to this problem was described in a previous paper (Waythomas et al., 2006), and the reader is referred to this work for
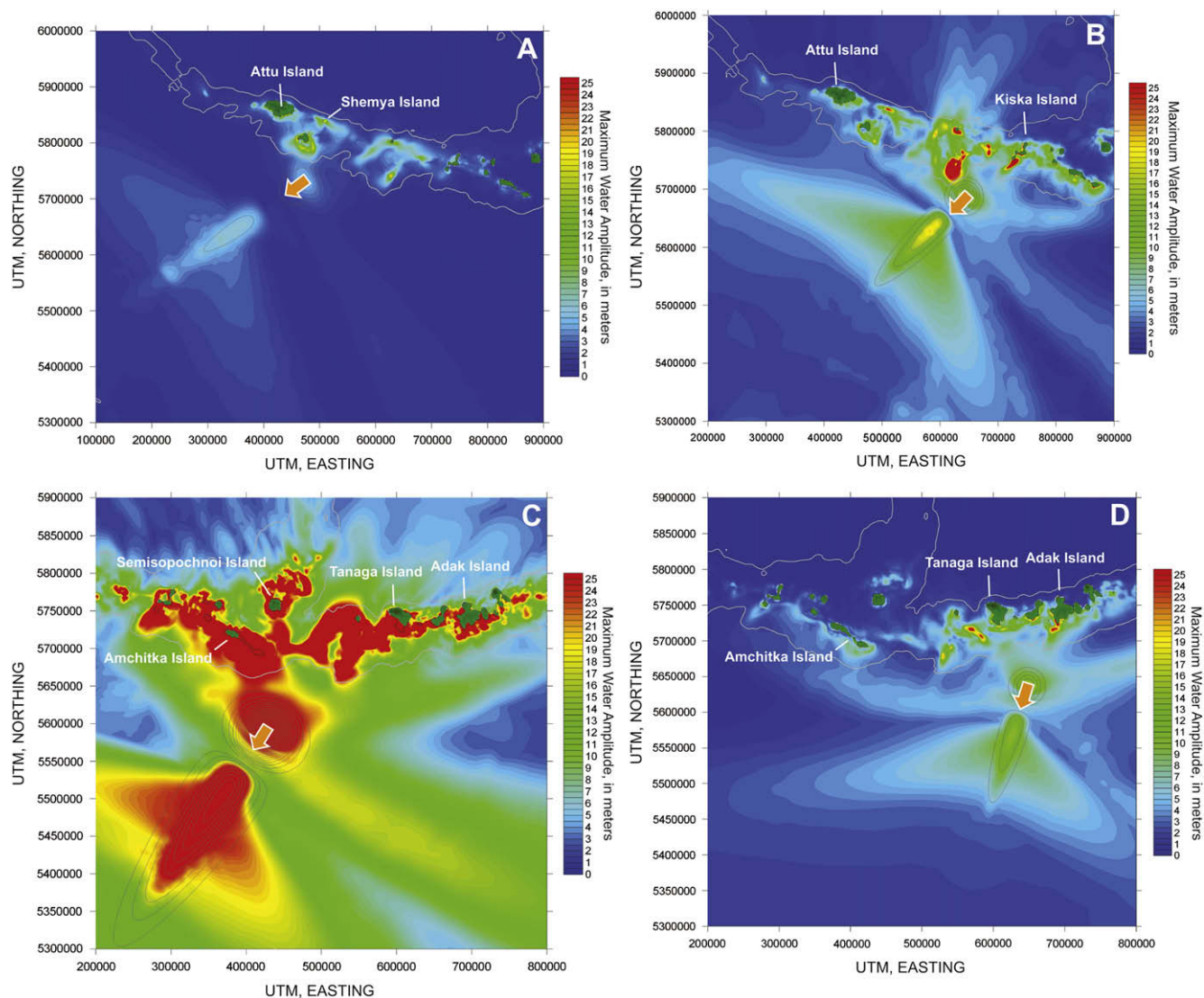
Fig. 3. Near-field maximum water elevations above sea level for hypothetical submarine mass flow tsunami sources. (A)–(D) Tsunami sources originating in submarine canyons; (E)–(H) tsunami sources originating on the trench slope. A, Heck Canyon source; B, Murray Canyon source; C, Amchitka Pass source; D, Adak Canyon source; E, Tanaga slope source; F, Sitkin slope source; G, Unimak slope source; H, Shumagin slope source.
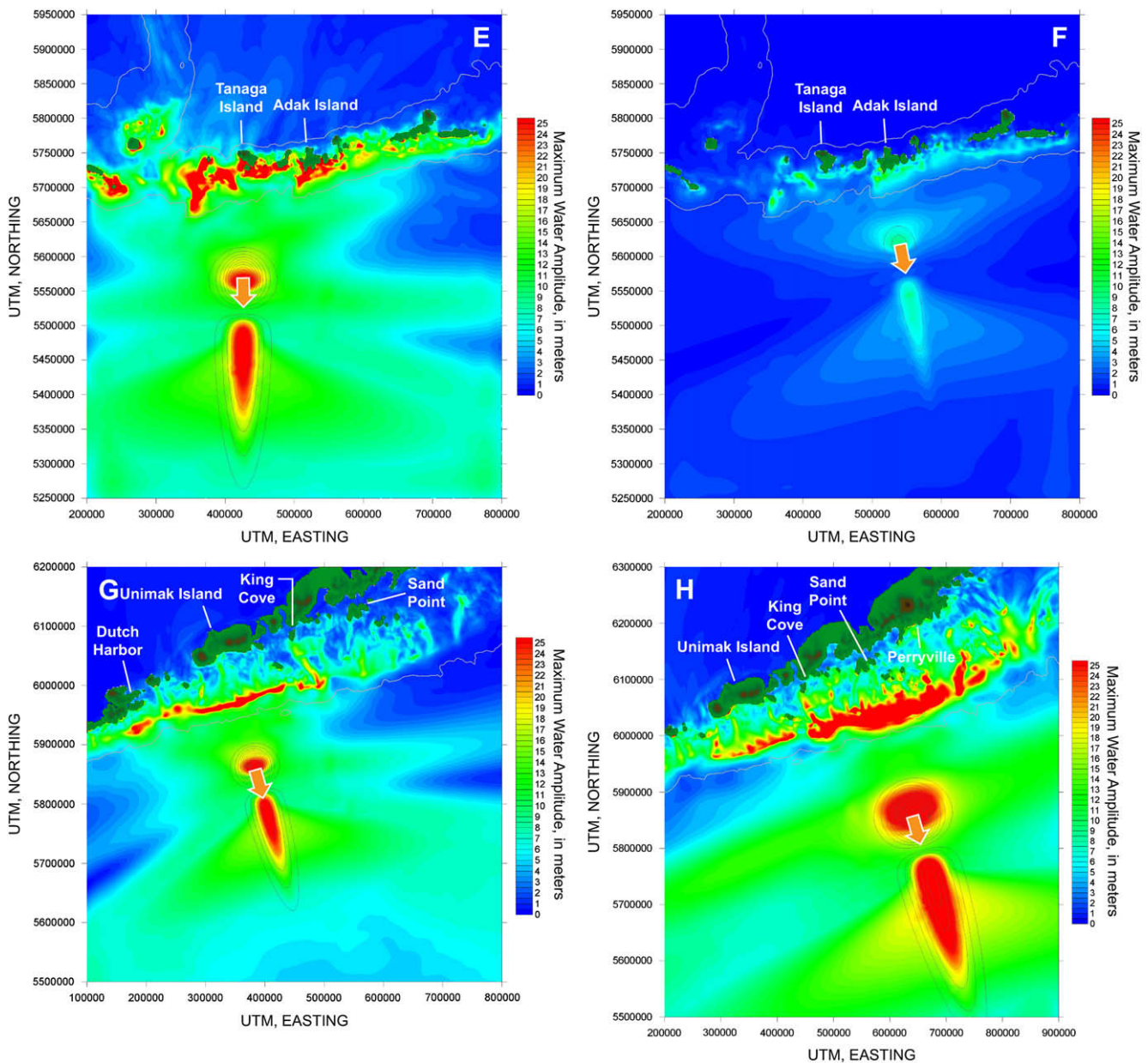
Fig. 3. (*continued*).

more information about our treatment of tsunami generation by debris avalanche.

Island volcanoes in the Aleutian arc and elsewhere are prone to lateral failures and this process is a well-known mechanism for tsunami generation (Keating and McGuire, 2000; McGuire, 2006). Although there have been no known historical flank failures at volcanoes in Alaska that resulted in tsunamis, except for Augustine Volcano (Waythomas et al., 2006), large scale flank collapse and debris avalanche runout into the sea has been documented at several Aleutian volcanoes (Waythomas et al., 2002, 2003a,b; Coombs et al., 2007). It is difficult to know beforehand how much of a volcanic edifice will be involved in a flank collapse. Evaluations of debris-avalanche deposits resulting from flank collapse indicate that most large-scale collapses involve about one-third or more of the total edifice volume (Siebert, 1996). Island volcanoes in the Aleutian arc have subaerial edifice volumes that range from about 0.5 km³ to about 200 km³ (Table 3). Assuming that the total edifice

volume is at least twice the subaerial volume, and one-third of this amount is a plausible volume for a potential flank collapse, large-scale lateral flank collapses at island volcanoes in Alaska could produce between 0.3 and 140 km³ of material. A volcanic debris avalanche with a volume in this range could be tsunamigenic, and, as we show later, far-field waves could be significant and local waves near the source could produce large runup on nearby islands and coastlines. We note that a tsunami may have been initiated when about 0.09 km³ of avalanche debris from Augustine Volcano entered Cook Inlet during an eruption in 1883 (Waythomas et al., 2006). This event indicates that large volumes of debris are not necessarily required to produce potentially hazardous waves, although the impact and damage of smaller events is limited in areal extent. Maximum tsunami wave elevations and depressions depend on other factors including debris flux, water depth, landslide Froude number, geometry, and no clear relation exists between landslide volume and maximum wave elevation (Murty,

2003). As we have suggested elsewhere, tsunami generation depends on the volume flux entering the water (Waythomas et al., 2006).

All of the known submarine debris-avalanche deposits associated with flank collapse in the Aleutian Islands entered the Bering Sea (Waythomas et al., 2002, 2003a,b; Coombs et al., 2007), but because the data needed to identify flank collapse debris-avalanche deposits in North Pacific settings are not available, we do not know how common such deposits are in this area. Thus, our evaluation of volcanic avalanches that enter the North Pacific is hypothetical, and available evidence indicates that avalanche-initiated waves, if they did form, have been directed primarily to the north.

5. Mass-flow motion

Mass-flow motion governs tsunami generation, and the acceleration phase of the flow during the early stages of a tsunamigenic mass-flow event has the greatest influence on initial wave elevation and tsunami generation (Watts, 1998, 2000; Watts et al., 2003, 2005). Mass-flow motion can be described by evaluating the balance of forces acting on the flow and applying standard equations of motion for center of mass displacement along the sea floor (Slingerland and Voight, 1979; Heinrich, 1992; Pelinovsky and Poplavsky, 1996; Watts, 1997; Watts and Grilli, 2003; Grilli and Watts, 2005). Deformation about the center of mass is addressed using the center of mass motion. We consider a gravity-driven mass flow moving down a finite, planar slope inclined at angle θ to the horizontal. The mass flow is treated as a deforming body, where deformation occurs relative to, and about, the center of mass motion $s(t)$. We subdivide the slope over which the mass flow moves into linear segments where each segment has a constant slope θ. The instantaneous velocity $u(t)$ of the mass flow for a given planar slope segment has the form:

$$\frac{du}{dt} \approx \frac{B}{A} - \frac{C}{A}u^2 \tag{1}$$

where the first term B/A represents both gravitational acceleration and the effect of bed friction, and the second term $(C/A)u^2$, represents drag by the ambient fluid (either air or water) at the center of mass location. The coefficients $A \equiv (\rho_b + C_m\rho_0)$, $B \equiv (\rho_b - \rho_0)g(\sin\theta - C_n\cos\theta)$, and $C \equiv \rho_0 C_d/2L$ are slowly varying functions of time (Watts, 1997, 1998, 2000). In the expressions for A, B, and C above, ρ_b is the instantaneous bulk density, ρ_0 is the ambient fluid density, C_m is the added mass coefficient, g is gravitational acceleration, C_n denotes the instantaneous Coulomb friction coefficient, C_d is the total drag coefficient, and L is the
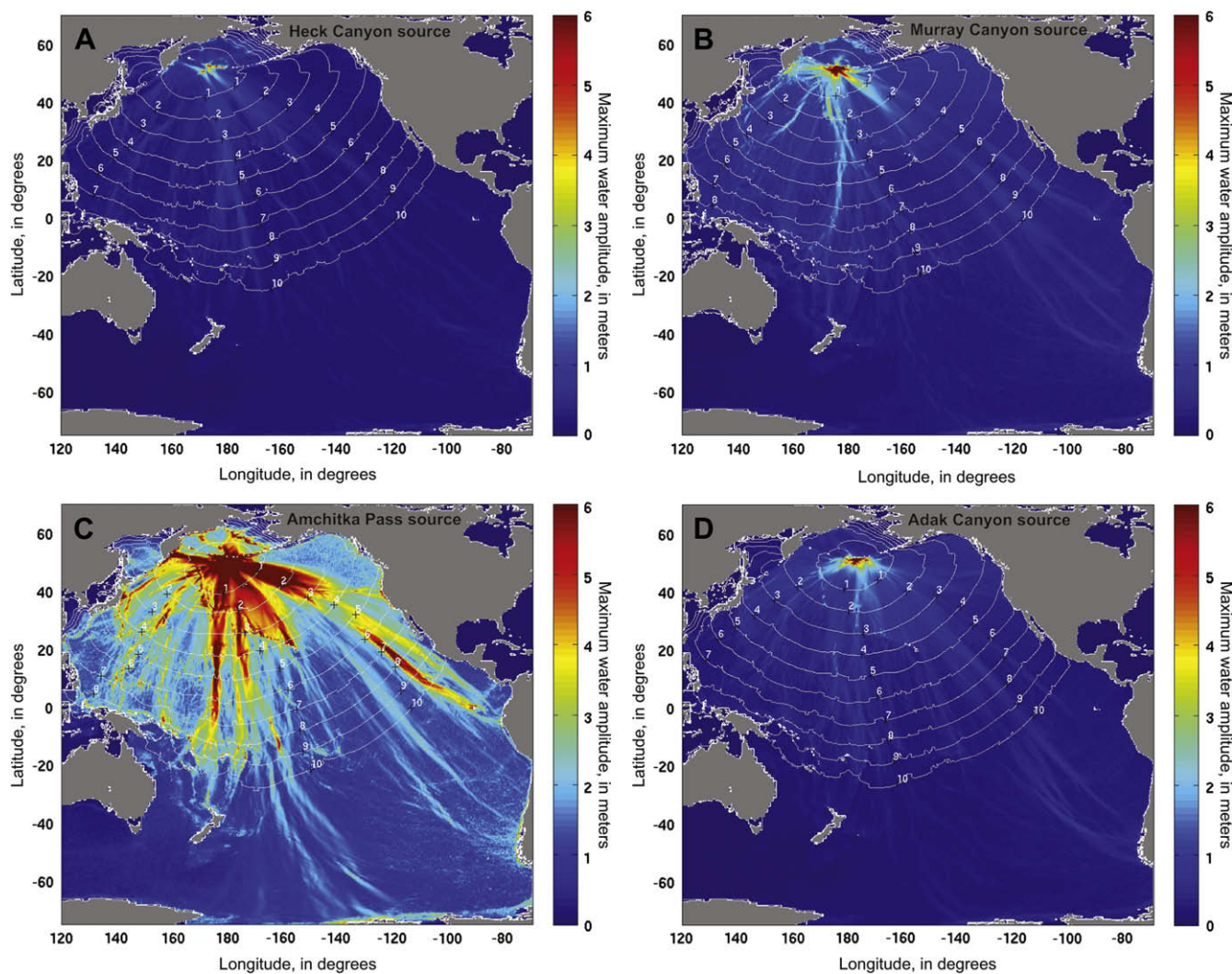
Fig. 4. Far-field maximum water elevation above sea level for hypothetical submarine mass-flow tsunami sources. A, Heck Canyon source; B, Murray Canyon source; C, Amchitka Pass source; D, Adak Canyon source; E, Tanaga slope source; F, Sitkin slope source, G, Unimak slope source; H, Shumagin slope source.
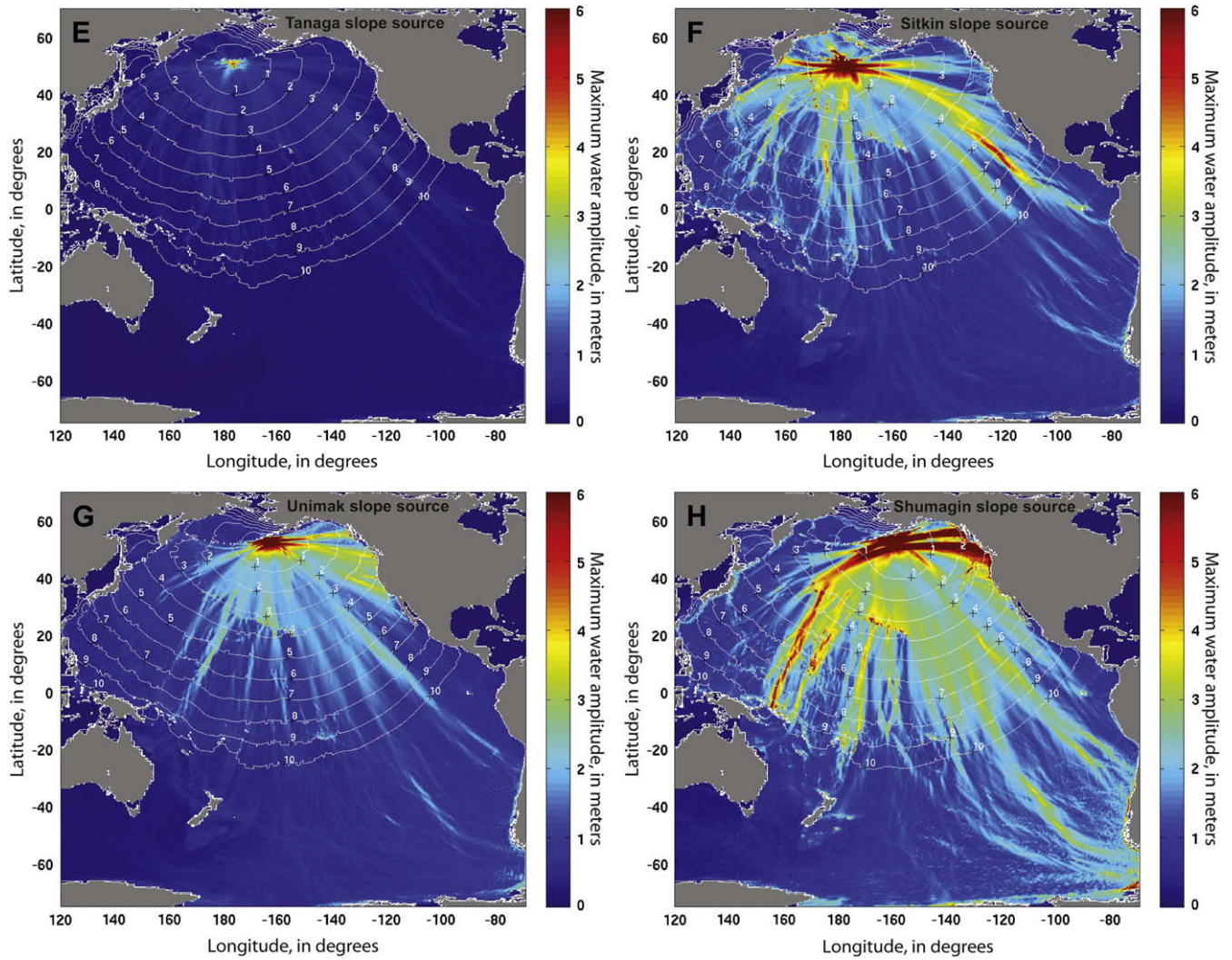
Fig. 4. (*continued*).

instantaneous mass flow length (see Watts, 1998, 2000; Grilli and Watts, 1999; Watts et al., 2000; Grilli et al., 2002; Brodsky et al., 2003; Enet et al., 2003; Watts and Waythomas, 2003). We set $C_m = 1.17$, $C_n = 0.01$, and $C_d = 1.44$ to perform the computations that utilize the coefficients A, B, and C. These are typical values for mass-flow motion calculations (Waythomas et al., 2006). We do not consider entrainment for these landslides.

We assume that mass-flow motion occurs over discrete time steps Δt, where $\Delta t = t - t_i$ is the time difference between the beginning and end of the time step, and with the initial condition $u(t_i) = u_i$. If the coefficient $B > 0$, the flow is accelerating and the mass-flow velocity changes according to:

$$u(t) \cong \sqrt{\frac{B}{C} \frac{\tanh\left[\sqrt{BC(t - t_i)}/A\right] + u_i\sqrt{C/B}}{1 + u_i\sqrt{C/B}\tanh\left[\sqrt{BC(t - t_i)}/A\right]}} \qquad (2)$$

We solve for position $s(t)$ along the slope by integrating the velocity $u(t)$ numerically over time, starting with $u_i = 0$ at $t_i = 0$. For a planar slope, we integrate Eq. (2) to find an analytical solution for center of mass position as a function of time. Doing so yields the familiar law of motion:

$$u(t) = s_0 \ln\left(\cosh\frac{t}{t_0}\right) \qquad (3)$$

where $s_0 = A/C$ and $t_0 = A/\sqrt{BC}$ are the characteristic distance and time of mass-flow motion, respectively (Watts, 1998; Watts et al., 2000; Grilli and Watts, 2001; Enet et al., 2003).

To account for deformation of the mass flow as it moves, internal deformation about the center of mass is parameterized in terms of the center of mass motion. The center of mass position $s(t)$ can be shifted down slope as internal deformation takes place, increasing the acceleration of the center of mass (Watts and Grilli, 2003). Similarly, the nose position $N(t)$ over time, and the mass-flow length as a function of time $L(t)$, increase in proportion to the center of mass motion $s(t)$. There are three dynamic deformation coefficients with values based on experimental results (Watts, 1997; Fritz, 2002), numerical analysis (Watts and Grilli, 2003; Locat et al., 2004), and case studies of mass-flow tsunami generation (Greene et al., 2006; Waythomas et al., 2006).

Mass-flow thickness with respect to time $H(t)$ can be estimated from conservation of mass, in simplified form:

$$H(t) \approx \frac{3V_i}{2L(t)W} \qquad (4)$$

where V_i is initial volume, $L(t)$ is instantaneous mass-flow length, and W is a typical mass-flow width, here assumed constant. The ratio 2/3 is a shape factor that relates the product of the length
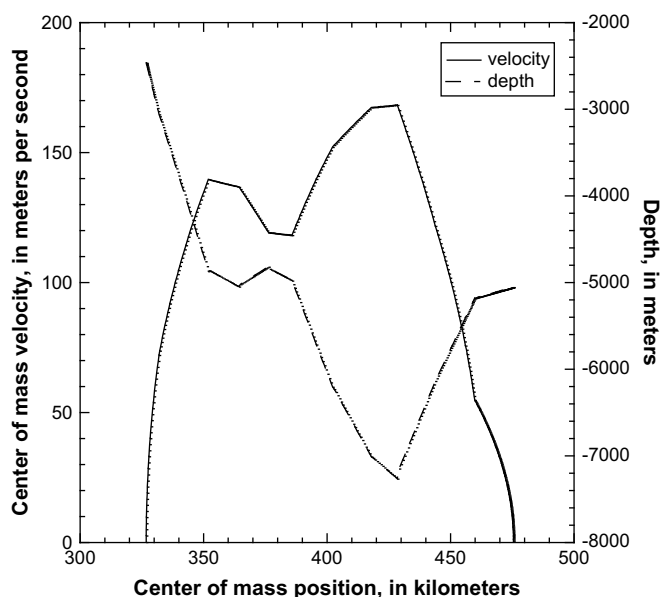
Fig. 5. Center-of-mass velocity versus position and bottom depth for the hypothetical Tanaga slope mass flow, which is typical of those evaluated in this paper. Location of depth profile shown in Fig. 6.

scales to the mass-flow volume. Mass-flow length with respect to time $L(t)$ is calculated with the following equation:

$$L(t) = L_i + C_{st}(s(t) - s_i) \qquad (5)$$

where L_i is the initial mass-flow length, C_{st} is a dynamic length coefficient (set to a value C_{st} of 0.35), and s_i is the initial mass-flow position. Center of mass motion $s(t)$ is the only other length scale available to modify mass-flow length in time. It could be said that the center of mass motion drives the deformation process. Mass-flow velocity with respect to time $U(t)$ is calculated using

$$U(t) = U_i + C_{at}(U(t) - U_i) \qquad (6)$$

where U_i is the initial center of mass velocity and C_{at} is a dynamic acceleration coefficient (set to a value of C_{at} 1.4). Eq. (6) amplifies changes in velocity due to mass-flow deformation. Eqs. (1)–(6) provide a complete description of mass flow motion and deformation. Additional discussion of these concepts can be found in Watts and Grilli (2003), Greene et al. (2006), and Waythomas et al. (2006).

6. Numerical simulation

The initial mass flow tsunami source is calculated using a software package called TOPICS (Tsunami Open and Progressive Initial Conditions System). The output is linked to a public-domain Boussinesq wave propagation model called FUNWAVE (Wei and Kirby, 1995; Wei et al., 1995) by way of a tsunami community model Geowave (Watts et al., 2003, 2005). FUNWAVE handles frequency dispersion in a manner that simulates deep-water waves, models the fluid mechanics of breaking waves, and simulates wave inundation.

Boussinesq equations are employed to describe the weakly dispersive propagation of nonlinear water waves (Kirby, 2003). Wave propagation simulations were carried out using FUNWAVE, which can perform simulations for a variety of model systems including nonlinear shallow water equations, weakly nonlinear Boussinesq equations, and fully nonlinear Boussinesq equations, using a predictor-corrector scheme described by Wei and Kirby (1995). Further information on algorithms for wave breaking, shoreline inundation, runup, and bottom friction can be found in Chen et al. (2000) and Kennedy et al. (2000). The near-field simulations use a uniform 2×2 km UTM grid. The far-field simulations were performed on a regular, spherical, 10×10 min grid, using a weakly nonlinear model equation based on depth-averaged horizontal velocity.

The far-field model equations, implementations, and tests are described by Kirby et al. (2004). In the derivation of the ocean scale spherical coordinate model, we introduce a parameter λ to characterize the horizontal scale of the tsunami wave, with the ratio h/λ representing the dispersion parameter, where h is water depth. Taking λ to characterize to the Earth's radius (representing the case where motions scale with ocean basin dimensions) leads to the usual shallow-water equations, with Coriolis terms retained as leading-order accelerations, as well as contributions from undifferentiated velocity products to advective terms. Taking λ to be on the order of tens of kilometers leads to a dispersion parameter that is small, but not vanishingly so. Retention of leading order terms in the dispersion parameter then leads to the Boussinesq model system. Coriolis terms are about the same order as weak dispersion terms, whereas the undifferentiated components of the advective acceleration are scaled out of the model system. The parameter λ is a means of introducing Coriolis terms into a Boussinesq structure.

The numerical simulation capabilities of FUNWAVE have been used to describe: (1) wave breaking during propagation and sometimes again during inundation; (2) dispersion during
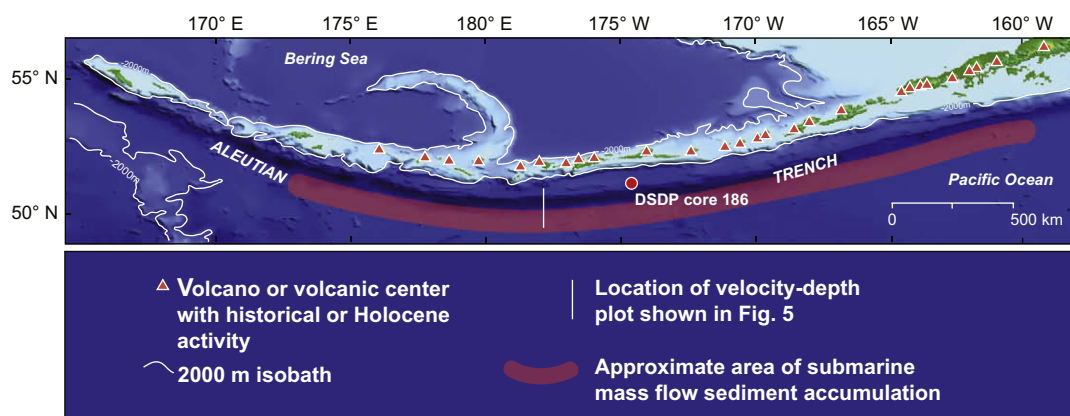
Fig. 6. Bathymetric map of the central and western Aleutian arc showing location of velocity-depth plot of Fig. 5, and approximate accumulation area for sediment deposited by submarine mass flows of the type we evaluate in this paper. Location of DSDP core 186, which contains submarine mass-flow deposits, is also indicated. Map location given in Fig. 2.

Table 1
Tsunami source parameters used and input for TOPICS.

Quantities	Heck Canyon	Murray Canyon	Amchitka Pass	Adak Canyon	Tanaga slope	Sitkin slope	Unimak slope	Shumagin slope
UTM longitude, x_o	552000	698000	488000	668000	426000	526000	360000	602000
UTM latitude, y_o	5781000	5744000	5676000	5704000	5674000	5686000	5950000	5998000
Flow path orientation, φ, in degrees	224	235	245	263	180	170	170	170
Mass flow specific density, γ	1.85	1.85	1.85	1.85	1.85	1.85	1.85	1.85
Initial mass flow length, b, in km	60	45	60	40	60	40	50	80
Maximum initial mass flow thickness, T, in m	600	450	600	400	600	400	500	800
Maximum mass flow width, w, in km	10	15	40	10	20	10	20	25
Mass flow volume, in km^3	360	300	1440	160	720	160	500	1600
Mean initial mass flow depth, d, in m	2200	2200	2600	2000	2400	3000	2000	2800
Flow path slope, θ, in degrees	2.3	5.1	4.6	5.7	4.6	5.7	4.6	4.0

propagation and the number of waves attacking the shoreline; (3) edge waves that interact with each other to produce the largest runup; and (4) accurate reproductions of measured runup and observed inundation (Watts et al., 2003; Waythomas and Watts, 2003; Fryer et al., 2004; Day et al., 2005; Waythomas et al., 2006; Ioualalen et al., 2007; Mattioli et al., 2007; Rahiman et al., 2007; Tappin et al., 2008). Nonlinear shallow water wave models used to simulate tsunami propagation and inundation have some difficulty in reproducing nearshore runup and inundation for most tsunami sources except long-wave earthquake tsunamis, and then most models have problems reproducing edge wave interactions and associated runup predictions. In our applications of FUNWAVE, we have found that the model has consistently reproduced wave observations and measurements for several case studies without need for any model adjustments or bathymetric corrections (e.g., Yeh et al., 1996; Watts et al., 2000; Tappin et al., 2008). FUNWAVE has been used successfully to perform simulations of relatively short waves generated by submarine and subaerial mass flows (Watts et al., 2003; Waythomas and Watts, 2003; Fryer et al., 2004; Day et al., 2005; Waythomas et al., 2006; Rahiman et al., 2007; Mattioli et al., 2007; Tappin et al., 2008) and relatively long waves resulting from co-seismic displacement (Day et al., 2005; Ioualalen et al., 2006, 2007; Grilli et al., 2007). We simulate plausible tsunami triggered by submarine landslides on both local and Pacific Ocean grids; however, we do not attempt detailed analysis of far-field effects because here we present only a preliminary examination of tsunami hazard.

7. Results

Near-field simulations of maximum water wave elevation for the submarine mass-flow initiated tsunamis are shown in Fig. 3, and initial wave properties are given in Table 4. These results indicate potential hazard zones for local waves in the Aleutian Islands and along the southern part of the Alaska Peninsula based on maximum water elevation. Although we do not report specific wave elevations for locations in the near-field region, we note that all of the mass flows originating in submarine canyons (Fig. 2) initiate tsunamis that could be hazardous to inhabited islands in the western Aleutians where wave elevations of >5 m are common (Fig. 3a–d). The largest waves result from a massive, but not unprecedented worldwide, mass flow (1440 km^3 in volume) that would produce wave elevations in excess of 20 m in the Adak-Amchitka sector of the Aleutian Islands (Fig. 3c). Several islands in this region are nearly engulfed by the tsunami, and wave inundation and coastal flooding are possible on northern shores of several islands including Adak and Adak harbor. Smaller mass flows in Heck Canyon, Murray Canyon, and Adak Canyon also produce significant local waves with maximum water elevations of >8 m (Fig. 3a,b,d).

Maximum near-field tsunami water elevations above sea level for mass flow tsunamis initiated by slope failures on the continental shelf are shown in Fig. 3e–h. All of the mass flows originating as slope failures on the shelf (Fig. 2) initiate tsunamis that also could be hazardous to inhabited islands in Aleutians and areas along the

Table 2
Examples of known or suspected tsunamigenic submarine mass flows and associated wave amplitudes and run-up heights if known (values in italics are calculated).

Location or event name and description	Volume, km^3	Maximum tsunami amplitude,[a] m	Maximum tsunami run up, m	Reference
Papua New Guinea, 1998	6-17	−25	10–15	Watts et al., 2003; Tappin et al., 2008
Grand Banks, 1929	200	Not known	4–8	Lander and Lockridge, 1989; McAdoo et al., 2003; Fine et al., 2005
Kitimat Inlet, BC, 1975	0.027	Not known	8.2	Murty, 1979; Skvortsov and Bornhold, 2007
Storegga 1	3880	40	20	Bugge et al., 1987, 1988; Bondevik et al., 2003, 2005
Alika 2	900	*940*	*800*	McMurtry et al., 2004
Nicoya Slump	1650	>27		von Huene et al., 2004
Fogo Island debris avalanche	250	Not known	Not known	Le Bas et al., 2007; Day et al., 1999
Oregon continental slope	800-900	*42*	Not known	Goldfinger et al., 2000; McAdoo and Watts, 2004
Suva, Fiji, 1953	0.06	−41	3-15, *8–10*	Rahiman et al., 2007
Arecibo slide, Puerto Rico	22		*15.7*	ten Brink et al., 2006
Kaikora Canyon, New Zealand	0.24	*13*	*20*	Walters et al., 2006
Southern California continental slope	0.5		*10–12*	Lee et al., 2004; Locat et al., 2004; Greene et al., 2006
Unimak Island, Alaska, continental slope	200	−61	*108*	Watts et al., 2003; Fryer et al., 2004
Skagway, Alaska, 1994	0.001-0.003	−17	11	Watts et al., 2003
Stromboli Island, Italy	0.02	~5	10	Tinti et al., 2006
Oshima-Oshima, Japan	2.5	Not known	Not known	Satake, 2007

[a] Maximum tsunami amplitude = vertical distance from trough to crest.

Table 3
Subaerial edifice and potential collapse volumes of island volcanoes in the Aleutian arc.

Volcano	Area, km^2	Summit altitude, km	Subaerial edifice volume,[a] km^3	Potential flank collapse volume, km^3	Likely tsunami source area
Kasatochi	5	0.314	0.5	0.3	Bering Sea or North Pacific Ocean
Adagdak	12	0.645	2.6	1.7	Bering Sea
Chagulak	8.5	1.142	3.2	2.2	Bering Sea or North Pacific Ocean
Kagamil	18	0.893	5.4	3.6	Bering Sea or North Pacific Ocean
Kanaga	23	1.307	10.0	6.7	Bering Sea
Segula	34	1.153	13.1	8.7	Bering Sea or North Pacific Ocean
Yunaska NE	81	0.55	14.8	9.9	Bering Sea or North Pacific Ocean
Yunaska SW	49	0.915	14.9	10.0	Bering Sea or North Pacific Ocean
Kiska	37	1.22	15.0	10.0	Bering Sea
Amukta	48	1.066	17.1	11.4	Bering Sea or North Pacific Ocean
Augustine	50	1.26	21.0	14.0	Cook Inlet
Carlisle	42	1.62	22.7	15.1	Bering Sea or North Pacific Ocean
Herbert	54	1.29	23.2	15.5	Bering Sea or North Pacific Ocean
Korovin	48	1.533	24.5	16.3	Bering Sea
Little Sitkin	63	1.188	24.9	16.6	Bering Sea
Cleveland	52	1.73	30.0	20.0	Bering Sea or North Pacific Ocean
Moffett	76	1.196	30.3	20.2	Bering Sea
Akutan	72	1.303	31.3	20.8	Bering Sea
Gareloi	66	1.573	34.6	23.0	Bering Sea or North Pacific Ocean
Tanaga (includes Sajaka cone)	68	1.806	40.9	27.3	Bering Sea
Seguam	201	1.054	70.6	47.0	Bering Sea or North Pacific Ocean
Great Sitkin	136	1.74	78.9	52.5	Bering Sea
Vsevidof	118	2.149	84.5	56.3	Bering Sea
Makushin	353	1.8	211.8	141.0	Bering Sea

[a] Volume estimates were made by digitizing the area of the edifice on 1:63,360 or 1:250,000 scale USGS topographic maps and then calculating volume using the standard formula for a cone. Total edifice volume is assumed twice that of the subaerial volume and the potential flank collapse volume is assumed to be one-third of the total volume.

North Pacific coast of the Alaska Peninsula. The Shumagin slope mass flow (1600 km^3 in volume; Fig. 2) produces the greatest water elevations (25 m), although the wave magnitude appears to dissipate as the leading wave evolves to a bore propagating in shallow water, and zones of high water maxima are less widespread (Fig. 3h). The Tanaga slope mass flow also produces a significant tsunami with water elevations >15 m in the vicinity of Adak Island (Fig. 3e). The smaller Sitkin and Unimak slope submarine landslides (Fig. 2) also produce significant waves, but areas of high water maxima are spatially limited (Fig. 3f,g).

Far-field simulations of maximum water elevation for the Pacific Ocean are shown in Fig. 4, and wave characteristics for three of the mass-flow sources are given 20 km or so offshore from selected locations around the Pacific Rim in Table 5. All of the mass flows produce transoceanic waves that could pose significant hazards to coastlines around the Pacific Ocean. Although we do not provide a detailed analysis of the runup and inundation effects of these waves, we note that maximum water elevations of several meters or more are possible at a number of locations around the Pacific Rim (Fig. 4). These offshore wave elevations are as large as, or larger than, those associated with the 2004 Sumatra tsunami approaching highly impacted regions such as Thailand or Sri Lanka. In addition, local runup values can be expected to be 2–3 times the offshore wave elevations in Table 5.

We apply our mass-flow motion equations to the Tanaga slide. Fig. 5 shows the velocity results from Eqs. (2) and (6), from which all other results are derived. The mass flow reaches a maximum velocity of around 170 m/s in the trench before coming to rest on the rise of the downgoing plate. The nose of the mass flow stops around 300 km farther south of the center of mass. These results are typical of all of the slides studied. We note that a turbidite shed from the top surface of the mass-flow would presumably travel even further south beyond the nose position, leaving a thin record of the event far out on the ocean floor. It is interesting that the mass-flow center of mass comes to rest near the highest region of the downgoing plate, suggesting that this is a sediment accumulation zone (Fig. 6). It is plausible that the rise itself consists of a thick pile of sediment eroded over geologic time. This hypothesis could be tested with available high resolution seismic tools.

We estimate the return period of the types of submarine mass flows we evaluate in this paper using the probabilistic model of Watts (2004). We chose an arbitrary time interval of 63,000 years and found that 32 submarine mass-flow events with volumes ≥100 km^3 produced tsunami elevations >10 m above sea level, with an average return period of about 2000 years over the entire Aleutian arc. These events could be initiated by earthquakes with moment magnitudes of 5.1–8.9 and can occur on slopes throughout the Aleutian arc margin. Given the low average sedimentation rate

Table 4
Calculated initial tsunami properties.

Calculated values	Heck Canyon	Murray Canyon	Amchitka Pass	Adak Canyon	Tanaga Slope	Sitkin Slope	Unimak Slope	Shumagin Slope
Mass flow acceleration, a_o, in m/s^2	0.1178	0.2609	0.2354	0.2915	0.2354	0.2915	0.2354	0.2047
Theoretical maximum mass flow velocity, u_{max}, in m/s	178	229	252	229	252	229	230	271
Characteristic distance of mass flow motion, s_o, in km	269	202	269	179	269	179	224	359
Characteristic time of mass flow motion, t_o, in s	1511	879	1069	784	1069	784	976	1324
Initial tsunami wavelength, λ_o, in km	222	129	171	110	164	135	137	219
Initial tsunami amplitude, η_o, in m	−19.3	−67.8	−179.1	−52.7	−108.3	−25.8	−107.2	−135.4

Table 5
Far field wave characteristics off selected Pacific Rim locations.

Location	Maximum amplitude, in meters	Wave period, min minutes	Arrival time, in hours
Heck Canyon mass flow			
Petropavlovsk, Russia	2.22	14	1.2
Tokyo, Japan	1.23	11	3.7
Hong Kong, China	0.31	14	7.2
Manila, Philippines	0.38	8	7.0
Nadi, Fiji	0.47	13	9.3
Aitape, PNG	0.37	17	7.6
Honolulu, USA	0.31	11	4.9
Papeete, Tahiti	0.2	12	9.8
Santiago, Chile	0.34	10	17.4
Los Angles, USA	0.17	15	6.5
Halmahera, Indonesia	1.48	15	6.3
Gisborn, New Zealand	0.14	14	11.8
Rio Gallegos, Argentina	0.05	65	20.3
Lima, Peru	0.19	10	15.1
Midway, USA	0.75	16	2.9
Unimak Slope mass flow			
Petropavlovsk, Russia	0.96	12	3.0
Tokyo, Japan	0.64	16	5.4
Hong Kong, China	0.14	12	8.8
Manila, Philippines	0.11	9	8.7
Nadi, Fiji	0.31	11	9.6
Aitape, PNG	0.25	11	9.1
Honolulu, USA	0.53	11	4.3
Papeete, Tahiti	0.79	11	8.9
Santiago, Chile	1.04	9	16.1
Los Angles, USA	2.42	10	5.0
Halmahera, Indonesia	0.64	11	6.8
Gisborn, New Zealand	0.7	11	11.9
Rio Gallegos, Argentina	0.11	62	19.0
Lima, Peru	0.49	10	13.7
Midway, USA	2.05	11	3.1
Shumagin Slope mass flow			
Petropavlovsk, Russia	0.59	22	3.3
Tokyo, Japan	2.91	13	5.8
Hong Kong, China	0.14	13	9.1
Manila, Philippines	0.49	10	9.0
Nadi, Fiji	1.19	10	10.0
Aitape, PNG	0.81	11	9.2
Honolulu, USA	1.06	17	4.2
Papeete, Tahiti	1.26	11	8.8
Santiago, Chile	2.06	11	15.9
Los Angles, USA	2.65	16	4.6
Halmahera, Indonesia	1.25	11	7.0
Gisborn, New Zealand	1.25	28	11.9
Rio Gallegos, Argentina	0.21	70	18.8
Lima, Peru	1.15	24	13.4
Midway, USA	2.89	18	3.2

Table 6
Tsunami source parameters for volcanic landslides.

Quantities	Makushin	Yunaska	Cleveland	Seguam
Submerged mass flow specific density, γ	1.95	1.95	1.95	1.95
Initial mass flow length, b, in km	36	13.2	10.2	15.9
Maximum initial mass flow thickness, T, in m	490	535	444	857
Maximum mass flow width, w, in km	18	8.7	7.7	9.3
Mass flow volume, in km^3	141	27.3	15.5	56.3
Mean initial mass flow depth, d, in m	3600	1320	1020	1590
Flow path slope, θ, in degrees	10.5	2.9	3.1	4.8

8. Discussion

Our numerical simulation results show that underwater mass flows in the Aleutian arc of Alaska can initiate large transoceanic tsunamis that could pose hazards to coastal regions around the Pacific Rim. We suggest that the southern slope of the Aleutian arc is an area conducive to the formation of potentially catastrophic landslide tsunamis, including those associated with large volcanic flank failures. Submarine mass flows large enough to produce Pacific-wide tsunamis could occur either on the continental slope or within submarine canyons. Although the hypothetical submarine mass flows we simulate have volumes greater than 100 km^3, this volume is not a lower limit for tsunami generation. Mass flows with volumes as small as 0.09 km^3 can initiate locally significant waves, as they did at Augustine Volcano (Waythomas et al., 2006). Currently available data do not define specific source regions for tsunamigenic submarine landslides based on documented deposits, scarps, or historical observations. However, we note that large submarine debris flows have been mapped on the north side of the Aleutian arc in GLORIA images of the sea floor (Groome et al., 1997). Thus, it seems reasonable to infer that similar mass flows do or can develop on the south flank of the arc because both flanks share the same source area. The events we simulate indicate the approximate size of submarine mass flows required to initiate waves large enough to be hazardous around the Pacific Rim. Our results could be useful for guiding future marine geophysical surveys in the region aimed at acquiring and interpreting sea floor imagery, sub-bottom profiles, cores, or other observations and samples. Our results also indicate significant local landslide tsunami hazards for the Aleutian Islands and parts of the southern Alaska Peninsula.

Although we do not specifically address volcanic flank failures at all Aleutian Island volcanoes as source mechanisms for tsunamis, our results indicate that volcanic flank failures involving >10 km^3 of material can initiate trans-oceanic tsunamis that are similar to, but slightly smaller than the submarine mass-flow tsunamis. The largest volcanic edifice in the region is that of Makushin Volcano on Unalaska Island (Fig. 2). This volcano has a subaerial edifice volume of about 200 km^3 and could have a total volume of at least twice this amount if the submarine roots of the volcano are included. Assuming that a typical large flank collapse may involve about one-third of the total edifice volume, a major flank collapse at Makushin could produce a debris avalanche with a volume of roughly 130 km^3, which is about the size of the smallest submarine mass flow we used in our numerical simulations (Table 1). Although the tsunami magnitude of a volcanic debris avalanche resulting from flank collapse is not strictly comparable to a similar-sized tsunamigenic submarine mass flow, the Sitkin slope mass-flow tsunami (Table 4) provides an approximation of the tsunami magnitude that could occur should a large (ca 130 km^3) volcanic flank collapse enter the North Pacific Ocean. The volume of such a collapse and

in the study region, the locations most likely to spawn large tsunamigenic submarine mass flows are those with low seismic return periods, thick rapidly accumulated sediment, or both.

We did not compute initial tsunami properties for all potential volcanic debris avalanches and flank collapses at Aleutian Island volcanoes. To illustrate the magnitude of potential tsunamigenic events associated with debris avalanches entering the sea, we chose four volcanoes involving large to intermediate avalanche volumes (Table 3). These volcanoes are Makushin, Seguam, Cleveland, and Yunaska (Fig. 2), and we simulate avalanches entering the North Pacific at Seguam, Cleveland, and Yunaska SW, and into the Bering Sea at Makushin (Table 6). Volcanic debris avalanches at all of these locations could produce waves (Table 7), and those entering the North Pacific are large enough to produce waves that travel across the Pacific Ocean. However, far-field waves from volcanic debris avalanche sources are not as large as those associated with the submarine mass flows described above.

Table 7
Calculated initial tsunami properties for selected volcanic landslides.

Calculated values	Makushin	Yunaska	Cleveland	Seguam
Mass flow acceleration, a_o, in m/s^2	0.91	0.18	0.24	0.39
Theoretical maximum mass flow velocity, u_{max}, in m/s	124	174	182	80
Characteristic distance of mass flow motion, s_o, in km	163	184	219	49
Characteristic time of mass flow motion, t_o, in s	2440	1802	2753	520
Initial tsunami wavelength, submarine component, λ_o, in km	101	70	53	66
Initial tsunami amplitude, submarine component, η_o, in m	−111	−18	−19	−62
Initial tsunami wavelength, subaerial component, λ_o, in km	126	130	165	17
Initial tsunami amplitude, subaerial component, η_o, in m	61	37	19	156

For these landslides, each begins as a subaerial mass flow, enters the sea, and then becomes a submarine mass flow. So we compute the initial tsunami amplitude and wavelength for both the subaerial and submarine components.

the resulting debris avalanche would need to be at least comparable to a mass flow with characteristics like the Sitkin slope mass flow, and would have to flow uninhibited along the sea floor into the North Pacific Ocean to initiate a tsunami that could be hazardous to coastlines around the Pacific Rim. With the exception of Makushin Volcano, all of the volcanoes in the Aleutian Islands have approximate edifice volumes that are less than about 85 km^3 and potential flank collapse volumes of about 55 km^3 or less (Table 3). Although flank failures involving volumes of this amount could lead to tsunami generation, we note that a majority of these events would involve north-directed failures into the Bering Sea whose coastlines are far less inhabited than those of the Pacific Ocean.

We reiterate that our analysis indicates that hazardous local, as well as transoceanic tsunamis can result from large submarine mass flows and volcanic landslides that originate on the south flank of the Aleutian arc. These results are testable but require marine geologic studies in the region to correctly identify and map submarine mass-flow deposits and features. Our results provide an indication of how large such deposits might be and thus could be used to develop an appropriate data collection strategy. The benefits of using a numerical model like Geowave are its ability to incorporate known or assumed geological phenomena as tsunami sources. Thus, bathymetric and nearshore topographic data obtained by future marine studies of the southern Aleutian arc could be easily incorporated into revised tsunami simulations. It is also possible to use the output from FUNWAVE to calculate various wave effects in runup and inundation areas, such as transport of sediment, wave timing, and wave forces on structures, boats, buildings and people (Walder et al., 2006; Waythomas et al., 2006). Although we do not attempt such calculations here, this approach would yield much improved tsunami hazard assessments in coastal areas at risk.

Finally we suggest that submarine and subaerial landslide-initiated tsunamis in the Aleutian Islands region could be a previously unrecognized hazard that requires further study and documentation. If future marine studies of the region indicate the presence of submarine mass-flow deposits and related features, such as scarps, slump blocks, and turbidites, it may be important to develop a warning system specifically designed to detect potentially tsunamigenic mass flows on the sea floor. At present, there is no such warning system in place, and existing tsunami warning systems are unable to detect or interpret the tsunami hazard described here especially for submarine mass flows not initiated by earthquakes or initiated by earthquakes with magnitude $M < 7$. The capability to correctly identify a landslide-initiated tsunami is critical so that highly damaging surprise events do not strike places like Hawaii or other vulnerable locations around the Pacific Ocean. The Aleutian Islands region of Alaska supports a large and economically significant international fishing fleet, and several of the ports in the region are among the largest commercial seaports in the world (e.g., Dutch Harbor/Unalaska). Many of these ports and a number of communities in the Aleutian

Islands could face potentially catastrophic local tsunamis that could cause significant damage to port facilities and coastal structures and installations. All of these areas could be effectively isolated from outside assistance in the event of an unheralded mass-flow tsunami. Thus, we encourage a new approach to tsunami warning, one that seeks to identify the source of tsunami generation, and one that includes the detection of landslide tsunamis.

9. Conclusions

We propose that the Aleutian arc poses previously unrecognized landslide tsunami hazards. Large underwater landslides have occurred along the northern slopes of the Aleutian arc margin and likely exist south of the arc. Our analysis suggests that a sediment accumulation zone exists south of the Aleutian trench. We simulate eight plausible tsunami generated by submarine landslides and four volcanic landslide tsunamis on both local and Pacific Basin grids. Our results demonstrate a range of consequences, but with one clear outcome: the Aleutian arc presents hazardous landslide tsunamis locally and around the Pacific Basin. We do not attempt to study the impact of any specific event, in this preliminary examination of tsunami hazard. All of the events we simulated, however, yield local runup along the nearest coastlines of 10–20 m above sea level, depending on the event. All of the events also produce transoceanic tsunamis with significant far-field damage potential, some more so than others. For some events, peak tsunami elevations in far-field locations around the Pacific Ocean reach are 2–3 m above sea level at distances up to 20 km from the shore. In some of these areas, local runup could be two times or more than this value depending on the geometry of the coastline and wave interactions. We suggest that potential hazards from mass-flow tsunamis in the Aleutian arc region could be better mitigated if a local tsunami warning system were deployed, as existing tsunami warning systems are not designed to detect or interpret this type of tsunami hazard.

References

Bondevik, S., Mangerud, J., Dawson, S., Dawson, A., Lohne, Ø., 2003. Record-breaking height for 8000-year-old tsunami in the North Atlantic. EOS 84, 293.
Bondevik, S., Løvholt, F., Harbitz, C., Mangerud, J., Dawson, A., Svendsen, J.I., 2005. The Storegga Slide tsunami – comparing field observations with numerical simulations. Marine and Petroleum Geology 22 (1–2), 195–208 (special issue).
Brodsky, E.E., Gordeev, E., Kanamori, H., 2003. Landslide basal friction as measured by seismic waves. Geophysical Research Letters 30 (24), doi:10.1029/2003GLO18485.

Bugge, T., Befring, S., Belderson, R.H., Eidvin, T., Jansen, E., Kenyon, N.H., Holtedahl, H., Sejrup, H.-P., 1987. A giant three-stage submarine slide off Norway. Geo-Marine Letters 7, 191–198.

Bugge, T., Belderson, R.H., Kenyon, N.H., 1988. The Storegga slide. Philosophical Transactions of the Royal Society. Series A 325 (1586), 358–390.

Carlson, P.R., Karl, H.A., Edwards, B.D., 1991. Mass sediment failure and transport features revealed by acoustic techniques, Beringian Margin, Bering Sea, Alaska. Marine Geotechnology 10 (1–2), 33–51.

Chen, Q., Kirby, J.T., Dalrymple, R.A., Kennedy, A.B., Chawla, A., 2000. Boussinesq modeling of wave transformation, breaking and runup, II: 2D. Journal of Waterway, Port, Coastal & Ocean Engineering ASCE 126, 48–56.

Coleman, J.M., Prior, D.B., 1988. Mass wasting on continental margins. Annual Review of Earth and Planetary Sciences 16, 101–119.

Coombs, M.L., White, S.M., Scholl, D.W., 2007. Massive edifice failure at Aleutian arc volcanoes. Earth and Planetary Science Letters 256 (3–4), 403–418.

Day, S.J., Heleno Da Silva, S.I.N., Fonseca, J.F.B.D., 1999. A past giant lateral collapse and present-day flank instability of Fogo, Cape Verde Islands. Journal of Volcanology and Geothermal Research 94 (1-4), 191–218.

Day, S.J., Watts, P., Grilli, S.T., Kirby, J.T., 2005. Mechanical models of the 1975 Kalapana, Hawaii earthquake and tsunami. Marine Geology 215 (1-2), 59–92.

Dobson, M.R., Karl, H.A., Vallier, T.L., 1996. Sedimentation along the fore-arc region of the Aleutian arc, Alaska. In: Gardner, J.V., Twichell, D.C., Field, M.E. (Eds.), Geology of the United States Seafloor: The View from GLORIA. Cambridge University Press, Cambridge, pp. 279–304.

Edgers, L., Karlsrud, K., 1982. Soil flows generated by submarine slides: case studies and consequences. In: Chryssostomomidis, C., Connor, J.J. (Eds.), Proceedings of the Third International Conference on the Behavior of Offshore Structures, pp. 425–437.

Enet, F., Grilli, S.T., Watts, P., 2003. Laboratory experiments for tsunamis generated by underwater landslides: comparison with numerical modeling. Proceedings of the 13th Offshore and Polar Engineering Conference 3, 372–379.

Engebretson, D.C., Cox, A., Gordon, R.G., 1985. Relative motions between oceanic and continental plates in the Pacific Basin. Geological Society of America Special Paper 206, 59.

Fine, I.V., Rabinovich, A.B., Bornhold, B.D., Thomson, R.E., Kulikov, E.A., 2005. The Grand Banks landslide-generated tsunami of November 18, 1929: preliminary analysis and numerical modeling. Marine Geology 215, 45–57.

Fournelle, J.H., Marsh, B.D., Myers, J.D., 1994. Age character, and significance of Aleutian arc volcanism. In: Plafker, G., Berg, H.C. (Eds.), The Geology of Alaska. The Geology of North America G-1. Geological Society of America, Boulder, CO, pp. 723–757.

Fritz, H.M., 2002. Initial phase of landslide generated impulse waves. PhD thesis, Swiss Federal Institute of Technology. Switzerland, Zurich.

Fryer, G.J., Watts, P., Pratson, L.F., 2004. Source of the great tsunami of 1 April 1946: a landslide in the upper Aleutian forearc. Marine Geology 203 (3–4), 201–218.

Geist, E.L., Childs, J.R., Scholl, D.W., 1988. The origin of summit basins on the Aleutian Ridge: implications for block rotation of an arc massif (Pacific). Tectonics 7 (2), 327–341.

Goldfinger, C., Kulm, L.D., McNeill, L.C., Watts, P., 2000. Super-scale failure of the southern Oregon Cascadia margin. Pure and Applied Geophysics 157, 1189–1226.

Greene, H.G., Murai, L.Y., Watts, P., Maher, N.A., Fisher, M.A., Paull, C.E., Eichhubl, P., 2006. Submarine landslides in the Santa Barbara Channel as potential tsunami sources. Natural Hazards and Earth System Sciences 6, 63–88.

Grilli, S.T., Watts, P., 1999. Modeling of waves generated by a moving submerged body. Applications to underwater landslides. Engineering Analysis with Boundary Elements 23, 645–656.

Grilli, S.T., Watts, P., 2001. Modeling of tsunami generation by an underwater landslide in a 3D numerical wave tank. Proceedings of the 11th Offshore and Polar Engineering Conference, 3, Stavanger, Norway, pp. 132-139.

Grilli, S.T., Watts, P., 2005. Tsunami generation by submarine mass failure. I: Modeling, experimental validation and sensitivity analyses. Journal of Waterways, Port. Coastal and Ocean Engineering 131 (6), 283–297.

Grilli, S.T., Vogelmann, S., Watts, P., 2002. Development of a 3D numerical wave tank for modeling tsunami generation by underwater landslides. Engineering Analysis with Boundary Elements 26 (4), 301–313.

Grilli, S.T., Ioualalen, M., Asavanant, J., Shi, F., Kirby, J., Watts, P., 2007. Source constraints and model simulation of the December 26, 2004 Indian Ocean Tsunami. Journal of Waterways, Port. Coastal and Ocean Engineering 133 (6), 414–428.

Groome, M.G., Gutmacher, C.E., Stevenson, A.J., 1997. Atlas of GLORIA sidescan-sonar imagery of the exclusive economic zone of the United States: EEZ-view. US Geological Survey Open File Report, 97–540.

Haeussler, P., Plafker, G., 2003. Earthquakes in Alaska. US Geological Survey Open-File Report, 95–624.

Hampton, M.A., Bouma, A.H., 1977. Slope instability near the shelf break, western Gulf of Alaska. Marine Geotechnology 2, 309–331.

Hampton, M.A., Lee, H.J., Locat, J., 1996. Submarine landslides. Reviews of Geophysics 34 (1), 33–59.

Harbitz, C.B., Løvholt, F., Pedersen, G., Masson, D.G., 2006. Mechanisms of tsunami generation by submarine landslides: a short review. Norsk Geologisk Tidsskrift 86 (3), 255–264.

Heinrich, P., 1992. Nonlinear water waves generated by submarine and aerial landslides. Journal of Waterways, Port. Coastal and Ocean Engineering 118 (3), 249–266.

Ioualalen, M., Pelletier, B., Watts, P., Regnier, M., 2006. Numerical modeling of the 26 November 1999 Vanuatu tsunami. Journal of Geophyscal Research 111, C06030, doi:10.1029/2005JC003249.

Ioualalen, M., Asavanant, J., Kaewbanjak, N., Grilli, S.T., Kirby, J.T., Watts, P., 2007. Modeling the 26th December 2004 Indian Ocean tsunami: case study of impact in Thailand. Journal of Geophysical Research 112, C07024, doi:10.1029/2006JC003850.

Jacob, K.H., Nakamura, K., Davies, J.N., 1977. Trench-volcano gap along the Alaska-Aleutian arc; facts and speculations on the role of terrigenous sediments. In: Talwani, M., Pitman III, W.C. (Eds.), Island Arcs, Deep Sea Trenches, and Back-Arc Basins. Maurice Ewing Series. American Geophysical Union, pp. 243–258.

Karl, H.A., Carlson, R., 1996. Alaskan EEZ. Geology of the United States' Seafloor. The View from GLORIA. Cambridge University Press, Cambridge, pp. 251–254.

Keating, B.H., McGuire, W.J., 2000. Island edifice failures and associated tsunami hazards. Pure and Applied Geophysics 157, 899–955.

Keefer, D.K., 1984. Landslides caused by earthquakes. Geological Society of America Bulletin 95 (4), 406–421.

Keefer, D.K., 2002. Investigating landslides caused by earthquakes – a historical review. Surveys in Geophysics 23 (6), 473–510.

Kennedy, A.B., Chen, Q., Kirby, J.T., Dalrymple, R.A., 2000. Boussinesq modeling of wave transformation, breaking, and runup. I: 1D. Journal of Waterway, Port. Coastal and Ocean Engineering 126 (1), 39–47.

Kirby, J.T., 2003. Boussinesq models and applications to nearshore wave propagation, surfzone processes and wave-induced currents. In: Lakhan, VC. (Ed.), Advances in Coastal Modeling. Elsevier, Amsterdam, pp. 1–41.

Kirby, J.T., Shi, F., Watts, P., Grilli, S.T., 2004. Propagation of short, dispersive tsunami waves in ocean basins. EOS Transactions of the AGU 85 (47) Abstract OS21E-02.

Lander, J.F., Lockridge, P.A., 1989. United States Tsunamis. US Department of Commerce, Publication 41–42.

Le Bas, T.P., Masson, D.G., Holtom, R.T., 2007. Slope failures of the flanks of the southern Cape Verde Islands. In: Lykousis, V., Sakellariou, D., Locat, J. (Eds.), Submarine Mass Movements and their Consequences. Springer, Berlin, pp. 337–345.

Lee, H.J., Kayen, R.E., Gardner, J.V., Locat, J., 2003. Characteristics of several tsunamigenic submarine landslides. In: Locat, J., Mienert, J. (Eds.), Submarine Mass Movements and their Consequences. Springer, Berlin, pp. 356–366.

Lee, H.J., Normark, W.R., Fisher, M.A., Greene, H.G., Edwards, B.D., Locat, J., 2004. Timing and extent of submarine landslides in Southern California, OTC Paper 16744. Proceedings. Offshore Technology Conference, Houston, TX.

Lee, H., Ryan, H., Kayen, R.E., Haeussler, P.J., Dartnell, P., Hampton, M.A., 2006. Varieties of submarine failure morphologies of seismically-induced landslides in Alaskan fjords. Norsk Geologisk Tidsskrift 86 (3), 221–230.

Locat, J., Mienert, J. (Eds.), 2003. Submarine Mass Movements and Their Consequences, 1st International Symposium. Kluwer Academic Publishers, pp. 509–519.

Locat, J., Lee, H.J., Locat, P., Imran, J., 2004. Numerical analysis of the mobility of the Palos Verdes debris avalanche, California, and its implication for the generation of tsunamis. Marine Geology 203 (3-4), 269–280.

Manley, W.F., Kaufman, D.S., 2002. Alaska paleoglacier atlas. Institute of Arctic and Alpine Research. University of Colorado. URL: http://instaar.colorado.edu/QGISL/ak_paleoglacier_atlas v.1.

Mattioli, G., Voight, B., Linde, A., Sacks, I.S., Watts, P., Widiwijayanti, C., Young, S.R., Hidayat, D., Elsworth, D., Malin, P.E., Shalev, E., Van Boskirk, E., Johnston, W., Sparks, R.S.J., Neuberg, J., Bass, V., Dunkley, P., Herd, R., Syers, T., Williams, P., Williams, D., 2007. Unique and remarkable dilatometer measurements of pyroclastic flow-generated tsunamis. Geology 35, 25–28.

McAdoo, B.G., Minder, J., Moore, A., Ruffman, A., 2003. Tsunami deposits from the 1929 Grand Banks earthquake and submarine landslide, Taylor's Bay, Newfoundland. Geological Society of America, Program and Abstracts, 32–4.

McAdoo, B.G., Watts, P., 2004. Tsunami hazard from submarine landslides on the Oregon continental slope. Marine Geology 203 (3–4), 235–245.

McGuire, W.J., 2006. Lateral collapse and tsunamigenic potential of marine volcanoes. In: Troise, C., DeNatale, G., Kilburn, C.R.J. (Eds.), Mechanisms of Activity and Unrest at Large Calderas. Geological Society of London, Special Publication 269, 121–140.

McMurtry, G.M., Watts, P., Fryer, G.J., Smith, J.R., Imamura, F., 2004. Giant landslides, mega-tsunamis, and paleo-sea level in the Hawaiian Islands. Marine Geology 203 (3–4), 219–233.

Miller, T.P., Smith, R.L., 1987. Late Quaternary caldera-forming eruptions in the eastern Aleutian arc, Alaska. Geology 15, 434–438.

Miller, T.P., McGimsey, R.G., Richter, D.H., Riehle, J.R., Nye, C.J., Yount, M.E., Dumoulin, J.A., 1998. Catalog of the historically active volcanoes of Alaska. US Geological Survey Open-File Report OF 98-0582 104pp.

Murty, T.S., 1979. Submarine slide-generated water waves in Kitimat Inlet, British Columbia. Journal of Geophysical Research 84 (C12), 7777–7779.

Murty, T.S., 2003. Tsunami wave height dependence on landslide volume. Pure and Applied Geophysics 160, 2147–2153.

Pelinovsky, E., Poplavsky, A., 1996. Simplified model of tsunami generation by submarine landslide. Physics and Chemistry of the Earth 21 (12), 13–17.

Piper, D.W., McCall, C., 2003. A synthesis of the distribution of submarine mass movements on the eastern Canadian margin. In: Locat, J., Mienert, J. (Eds.), Submarine Mass Movements and Their Consequences. Kluwer Academic Press, Dordrecht, pp. 291–298.

Rahiman, T.I.H., Pettinga, J.R., Watts, P., 2007. The source mechanism and numerical modeling of the 1953 Suva tsunami, Fiji. Marine Geology 237 (1–2), 55–70.

Satake, K., 2007. Volcanic origin of the 1741 Oshima-Oshima tsunami in the Japan Sea. Earth. Planets and Space 59 (5), 381–390.

Schaefer, J., Nye, C.J., 2002. Historically active volcanoes of the Aleutian Arc. Alaska Division of Geological and Geophysical Surveys Miscellaneous Publications, MP 0123, 1 sheet, scale 1:3,000,000.

Scholl, D.W., Vallier, T.L., Stevenson, A.J., Scholl, D.W., Grantz, A., Vedder, J.G., 1987. Geologic evolution and petroleum geology of the Aleutian Ridge. In: Geology and Resource Potential of the Continental Margin of Western North America and Adjacent Ocean Basins – Beaufort Sea to Baja California. Circum-Pacific Council for Energy and Mineral Resources, vol. 6, pp. 123–155.

Schwab, W.C., Lee, H.J., 1983. Geotechnical analysis of submarine landslides in glacial sediment, northeast Gulf of Alaska. In: Molnia, B.F. (Ed.), Glacial–Marine Sedimentation. Plenum, New York, p. 145.

Siebert, L., 1996. Hazards of very large volcanic debris avalanches and associated eruptive phenomena. In: Scarpa, R., Tilling, R.I. (Eds.), Monitoring and Mitigation of Volcano Hazards. Springer-Verlag, Berlin, pp. 541–572.

Simkin, T., Siebert, L., 1994. Volcanoes of the World, second ed. Geoscience Press, Tucson, AZ, 349 pp.

Skvortsov, A., Bornhold, B., 2007. Numerical simulation of the landslide-generated tsunami in Kitimat Arm, British Columbia, Canada, 27 April 1975. Journal of Geophysical Research 112 (2), F02028, doi:10.1029/2006JF000499.

Slingerland, R.L., Voight, B., 1979. Occurrences, properties and predictive models of landslide-generated impulse waves. In: Voight, B. (Ed.), Rockslides and Avalanches 2. Elsevier, Amsterdam, pp. 317–397.

Solheim, A., Berg, K., Forsberg, C.F., Bryn, P., 2005. The Storegga Slide complex: repetitive large scale sliding with similar cause and development. Marine and Petroleum Geology 22 (1–2), 97–107.

Taber, J.J., Billington, S., Engdahl, E.R., 1991. Seismicity of the Aleutian arc. In: Slemmons, D.B., Engdahl, E.R., Zoback, M.R., Blackwell, D.D. (Eds.), Neotectonics of North America, Decade Map, vol. 1. Geological Society of America, Boulder, CO, pp. 29–46.

Tappin, D.R., Watts, P., McMurtry, G.M., Lafoy, Y., Matsumoto, T., 2001. The Sissano, Papua New Guinea tsunami of July 1998–offshore evidence on the source mechanism. Marine Geology 175 (1–4), 1–23.

Tappin, D.R., Watts, P., Grilli, S.T., 2008. The Papua New Guinea tsunami of 1998: anatomy of a catastrophic event. Natural Hazards and Earth System Sciences 8, 243–266.

ten Brink, U.S., Geist, E.L., Andrews, B.D., 2006. Size distribution of submarine landslides and its implication to tsunami hazard in Puerto Rico. Geophysical Research Letters 33, L11307.

Tinti, S., Pagnoni, G., Zaniboni, F., 2006. The landslides and tsunamis of the 30th of December, 2002 in Stromboli analysed through numerical simulations. Bulletin of Volcanology 68, 462–479.

Underwood, M.B., 1986a. Sediment provenance within subduction complexes—an example from the Aleutian forearc. Sedimentary Geology 51, 57–73.

Underwood, M.B., 1986b. Transverse infilling of the central Aleutian Trench by unconfined turbidity currents. Geo-Marine Letters 6, 7–13.

Underwood, M.B., Hathon, E.G., 1989. Provenance and dispersal of muds south of the Aleutian arc, north Pacific Ocean. Geo-Marine Letters 9 (2), 67–75.

Vallier, T.L., Scholl, D.W., Fisher, M.A., Bruns, T.R., Wilson, F.H., Von Huene, R., Stevenson, A.J., 1994. The Geology of Alaska: Chapter 11, Geologic Framework of the Aleutian Arc. Geological Society of America, Boulder, CO, 1055 pp.

von Huene, R., Ranero, C.R., Watts, P., 2004. Tsunamigenic slope failure along the Middle America Trench in two tectonic settings. Marine Geology 203, 303–317.

Walder, J.S., Watts, P., Waythomas, C.F., 2006. Case study: mapping tsunami hazards associated with debris flow into a reservoir. Journal of Hydraulic Engineering 132 (1), 1–11.

Walters, R., Barnes, P., Lewis, K., Goff, J.R., Fleming, J., 2006. Locally generated tsunami along the Kaikoura coastal margin: Part 2. Submarine landslides. New Zealand Journal of Marine and Freshwater Research 40, 17–28.

Ward, S.N., 2001. Landslide tsunami. Journal of Geophysical Research 106, 11201–11215.

Watts, P., 1997. Water waves generated by underwater landslides, PhD thesis, California Institute of Technology, Pasadena, CA.

Watts, P., 1998. Wavemaker curves for tsunamis generated by underwater landslides. Journal of Waterway, Port, Coastal and Ocean Engineering 124 (3), 127–136.

Watts, P., 2000. Tsunami features of solid block underwater landslides. Journal of Waterway, Port, Coastal and Ocean Engineering 126 (3), 144–152.

Watts, P., 2004. Probabilistic predictions of landslide tsunamis off Southern California. Marine Geology 203, 281–301.

Watts, P., Grilli, S.T., 2003. Tsunami generation by deformable underwater landslides, in: Proceedings of the 13th Offshore and Polar Engineering Conference, pp. 364–371.

Watts, P., Waythomas, C.F., 2003. Theoretical analysis of tsunami generation by pyroclastic flow. Journal of Geophysical Research 108, 2563.

Watts, P., Imamura, F., Grilli, S.T., 2000. Comparing model simulations of three benchmark tsunami generation cases. Science of Tsunami Hazards 18 (2), 107–123.

Watts, P., Grilli, S.T., Kirby, J.T., Fryer, G.J., Tappin, D.R., 2003. Landslide tsunami case studies using a Boussinesq model and a fully nonlinear tsunami generation model. Natural Hazards and Earth System Science 3 (5), 391–402.

Watts, P., Grilli, S.T., Tappin, D.R., Fryer, G.J., 2005. Tsunami generation by submarine mass failure. II: Predictive equations and case studies. Journal of Waterway, Port, Coastal and Ocean Engineering 131 (6), 298–310.

Waythomas, C.F., Neal, C.A., 1998. Tsunami generation by pyroclastic flow during the 3500-year B.P. caldera-forming eruption of Aniakchak volcano, Alaska. Bulletin of Volcanology 60 (2), 110–124.

Waythomas, C.F., Watts, P., 2003. Numerical simulation of tsunami generation by pyroclastic flow at Aniakchak Volcano, Alaska. Geophysical Research Letters 30 (14) OCE 5-1-5-4.

Waythomas, C.F., Miller, T.P., Nye, C.J., 2002. Preliminary volcano-hazard assessment for Kanaga Volcano, Alaska. US Geological Survey Open-File Report OF 02-0397 1, sheet, 27 pp.

Waythomas, C.F., Miller, T.P., Nye, C.J., 2003a. Preliminary volcano-hazard assessment for Great Sitkin Volcano, Alaska. US Geological Survey Open-File Report OF 03-0112 1, sheet, 25 pp.

Waythomas, C.F., Miller, T.P., Nye, C.J., 2003b. Geology and late quaternary eruptive history of Kanaga Volcano, a calc-alkaline stratovolcano in the western Aleutian Islands, Alaska. US Geological Survey Professional Paper No. 1678, pp. 181–197.

Waythomas, C.F., Watts, P., Walder, J.S., 2006. Numerical simulation of tsunami generation by cold volcanic mass flows at Augustine Volcano, Alaska. Natural Hazards and Earth System Science 6 (5), 671–685.

Wei, G., Kirby, J.T., 1995. Time-dependent numerical code for extended Boussinesq equations. Journal of Waterway, Port, Coastal & Ocean Engineering ASCE 121 (5), 251–261.

Wei, G., Kirby, J.T., Grilli, S.T., Subramanya, R., 1995. A fully nonlinear Boussinesq model for surface waves. Part 1. Highly nonlinear unsteady waves. Journal of Fluid Mechanics 294, 71–92.

Wilson, B.W., Torum, A., 1972. Effects of tsunamis: An engineering study. In, the Great Alaska Earthquake of 1964. Oceanography and Coastal Engineering volume, 361–523. pp.

Wood, C.A., Kienle, J. (Eds.), 1990. Volcanoes of North America. Cambridge University Press, Cambridge, United States and Canada, 354 pp.

Yeh, H.H., Liu, P.L., Synolakis, C.E. (Eds.), 1996. Long-wave Runup Models. World Scientific, Singapore, 403 pp.